UCRL-ID-147181

Final Report – Effect of Magnetic Configuration on Spheromak Performance FY2000 – FY2001 Tracking #00-SI-008

D.N. Hill, E.B. Hooper, H.S. McLean, B.W. Stallard, S. Woodruff, and R.D. Wood

January 2002

U.S. Department of Energy

Lawrence
Livermore
National
Laboratory

1 DISCLAIMER

Work performed under the auspices of the U. S. Department of Energy by the University of California Lawrence Livermore National Laboratory under Contract W-7405-Eng-48.

Final Report

Effect of Magnetic Configuration on Spheromak Performance

FY 2000 – FY 2001

Tracking # 00–SI–008

Principal Investigator: D.N. Hill

Funding: FY2000 $720k
FY2001 $525k

Report Outline

1. Executive Summary
2. Research Goals
3. Overview of the SSPX Spheromak
   3.1 Bias coil installation
   3.2 Bias coil operation
4. Experimental results

Appendix 1. Selected References

Appendix 2. Collaborations

1. Executive Summary

This is the final report on LDRD SI-funded research to determine the Effect of Magnetic Field Configurations on Spheromak Performance for the years FY2000–FY2001, during which a new set of bias magnetic field coils was used to change the vacuum magnetic field configuration of the SSPX spheromak at LLNL. The USDOE Office of Fusion Energy Science funded the routine operation of the SSPX facility during FY00 and FY01. A photo of the SSPX facility as it appeared in mid-FY01, appears in Fig. 1 below. The main distinctive feature of the spheromak is that currents in the plasma itself produce the confining toroidal magnetic field, rather than a complex set of external coils.

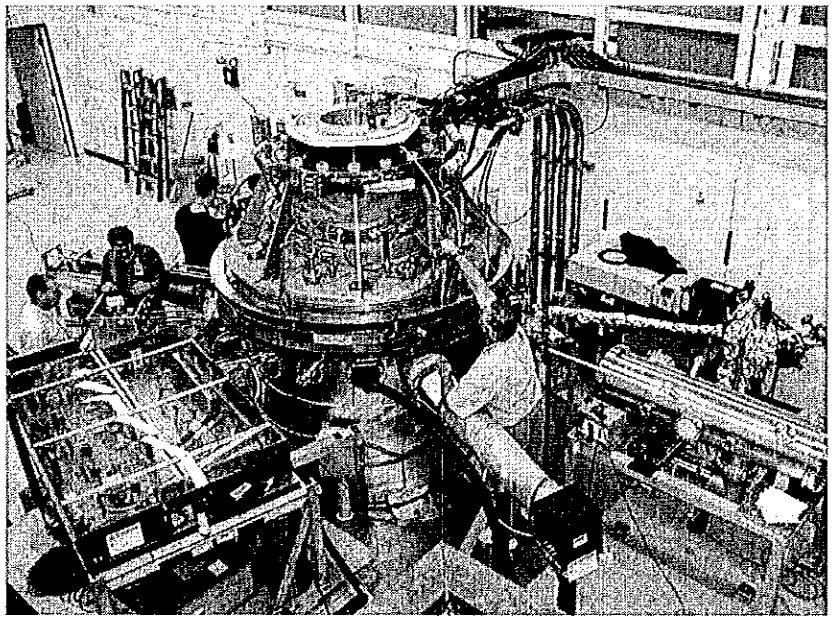

Fig. 1. Photograph of the SSPX device at LLNL in mid-FY2000. External components are plasma diagnostics.

The Sustained Spheromak Physics Experiment (SSPX) device was designed and built to study how well the spheromak can contain plasma energy while dynamo processes in the plasma maintain the confining magnetic fields. The spheromak potentially offers advantages over other fusion reactor concepts because it is compact, has no field coils linking the vacuum vessel, and can be operated in a steady state with voltage applied to external electrodes. It is predicted that the ability of the SSPX to contain the plasma thermal energy will increase with increasing plasma electron temperature; that is, the hotter it is, the better it will work. Our near-term goal for the SSPX facility is to determine which of several magnetic field

configurations works best to produce hot, well-confined spheromak plasmas. We also want to verify the predicted inverse relation between plasma temperature and heat loss, and to use these results to design an even higher-temperature follow-on experiment that will push closer to fusion conditions. New features of the SSPX spheromak include a large-radius coaxial plasma injector to improve efficiency, a conformal flux conserver to minimize open field lines around the plasma, a divertor to aid in cold-particle exhaust, and the programmable-bias magnetic field coils to vary the magnetic geometry. The effect of operating SSPX with the bias magnetic-field coils is the subject of this LDRD research project.

During FY2000 we installed and commissioned the set of six independently controllable bias magnetic field coils labeled 4 – 9 in Fig. 2 below.

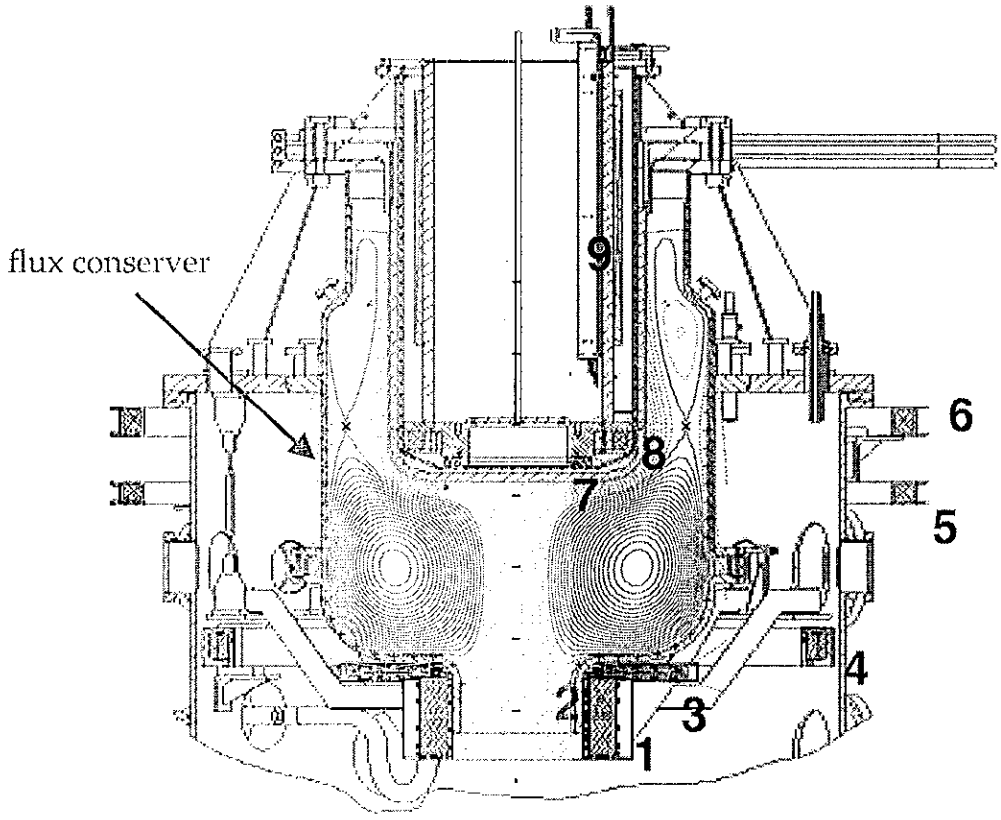

Fig. 2. Cross section of the SSPX spheromak device. Plasma magnetic flux surfaces in purple, bias coils in blux with coils labels. New coils are4 –9.

Four of these coils are located inside the SSPX vacuum vessel and have vacuum jackets and water cooling for heat removal. These coils are powered by high current (800A) DC power supplies that were obtained from previous experiments at LLNL. The coil currents are ramped up over a 25sec period to allow the magnetic fields to soak through the 2cm thick

copper flux-conserver shell of SSPX, which is also shown. During the course of testing the coils after installation, a water leak in a cooling line for one of the coils in vacuum was discovered and repaired. Otherwise, the coils and power supplies have performed according to their design specifications for over 2500 plasma pulses.

The bias coils, along with an original set of three injector magnetic field coils, provide an initial seed magnetic field that is twisted and amplified by currents driven through the spheromak plasma by an external capacitor bank. The complete coil set gives us unprecedented flexibility in studying how the geometry of the initial vacuum field in the SSPX spheromak affects plasma formation and magnetic field amplification. This configurational flexibility is one of the unique features of the SSPX spheromak.

Operation of SSPX with the bias coils commenced in FY2001. Experiments have shown that the new coils greatly expand the density range over which good spheromak plasmas can be formed in SSPX. This results from their ability to create an initial Penning discharge during spheromak formation, so that plasma discharges can be initiated with low gas pressure. Thus, we have found it possible to reduce the plasma density by factors of 2 to 3 and to increase the plasma electron temperature by similar factors. Lower plasma density reduces impurity radiation losses and allows the plasma temperature to rise without exceeding the fundamental pressure limits of the spheromak configuration. Besides representing record high temperatures in driven spheromak plasmas, these data show that SSPX can operate with a normalized plasma pressure of 5–10%, comparable to Tokamaks and other toroidal magnetic fusion devices.

We have made an initial comparison of six magnetic field configurations using the new bias field coils. These configurations fall into two categories: those with vacuum magnetic field lines lying parallel to the side walls of the SSPX chamber and those with diverging fields passing through the side walls of the chamber. Basic spheromak theory and SSPX data obtained before the installation of the bias coils suggested that up to three times higher field amplification could be expected with the field lines parallel to the walls. Contrary to predictions, however, we observed no increase in amplification with the parallel field. Surprisingly, we observed about 20% higher field amplification with the diverging magnetic field configuration than with the initial fields parallel to the walls everywhere in the flux conserver. We believe that these differences lie in the detailed path of current flow during early formation and the resulting magnetohydrodynamic stability of the resulting current channel.

In FY2002, with funding from the DOE Office of Fusion Energy Science, we will continue using the bias coils to examine how current amplification depends on the vacuum magnetic field geometry. We plan to install new diagnostics to better measure radiation losses and the distribution of plasma current, and to upgrade our density measurements.

2. Research Goals

The primary attractive feature of the spheromak as a magnetic fusion energy reactor concept is that currents in the plasma itself produce the confining toroidal magnetic field, rather than by external coils which necessarily thread the vacuum vessel in devices like the tokamak. This could lead to smaller, cheaper power plants. The magnetic geometry of the spheromak is shown in the cartoon of Fig. 3: the overall geometry is toroidal, like a donut, but with a very small hole in the middle [1].

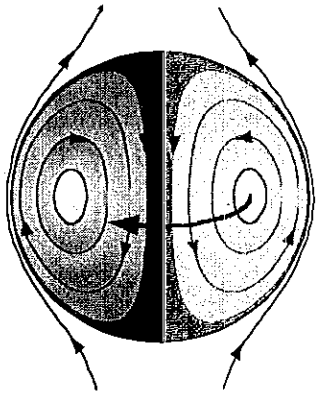

Fig. 3. Basic geometry of the spheromak configuration. Arrows indicate direction of magnetic field lines and plasma current. Blue arrow indicates toroidal direction, black arrows the poloidal direction.

Around the edge the magnetic fields are poloidal (threading the donut hole) and in the middle they are toroidal (direction indicated by the heavy blue arrow). This configuration (called a Taylor state) is force-free (i.e., $\nabla\times\mathbf{B}=\lambda\mathbf{B}$, λ=constant) so that the magnetic fields and plasma currents are aligned [2]. While spheromaks are relatively easily formed, full understanding of the underlying formation processes is still lacking. Consequently, there are three main areas of uncertainty relating to potential spheromak performance as a magnetic fusion reactor:

1. Is there sufficient energy confinement (can it hold heat)?
2 Can the configuration hold adequate plasma pressure (against pressure driven MHD modes)?
3 Can the magnetic configuration be actively controlled with external coils (against MHD tilt and shift modes)?

The central issue of energy confinement in spheromaks is tied to the fundamental mechanism that produces the force-free field configurations (the Taylor states) characteristic of these devices, namely both ideal and resistive MHD modes. The transport of helicity (interconnected flux) into the core of the spheromak, and the dynamo action underlying the transport, are thought to be due to resistive "tearing" modes in the plasma. These modes break axisymmetry (as required by Cowling's theorem [3] for the dynamo), and are closely related to magnetic reconnection events, for example in the tail of the magnetosphere and on the surface of the sun. They result when dissipative processes, typically in a thin "reconnection" layer, allow the magnetic field to find a lower energy state. When there are multiple modes undergoing this process, magnetic turbulence results. One consequence is the opening of the equilibrium magnetic surfaces, allowing energy to leak from the spheromak core to the edge.

The bias magnetic field coils provide control of the initial vacuum seed magnetic field. The vacuum field with and without the bias coils is shown in Fig. 4. In the reference case, the spheromak is formed when the plasma current in the injector (the coaxial region above z=0.25m in Fig. 4) exceeds the threshold value needed to bend the vacuum field lines down into the flux conserver region (the "pillbox-like" region with R=0.5m below z=0.25m in Fig. 4). In the standard configuration, the condition for ejecting plasma from the injector and forming the spheromak is that the toroidal magnetic field produced by current flowing along the inner electrode (see Fig. 2 above), exceed the initial vacuum magnetic field strength. Formally, this threshold condition [4] is $\lambda_g = \mu_0 I_g / \phi_g > \lambda_{crit}$, where I_g is the injector current and ϕ_g is the vacuum flux, and $\lambda_{crit} = \pi/\Delta = 20m^{-1}$ in SSPX. Once the plasma and field is ejected from the coaxial injector region, magnetic field can begin to build in the flux conserver as long as $\lambda = \mu_0 j/B \geq \lambda_{FC}$, the flux conserver geometrical eigenvalue for the force-free Taylor state. The flux conserver eigenvalue, λ_{FC} is set by the geometry of the flux conserver region: $\lambda_{FC}=9.9m^{-1}$ for SSPX. Thus, for SSPX, we have $\lambda_{crit} \approx 2\times\lambda_{FC}$ in the standard configuration. In the bias coil configuration, magnetic field lines already thread the flux conserver region and the threshold is reduced to $\lambda_g \geq \lambda_{FC}$, or about a factor of two. This should allow us to form and sustain the spheromak much closer to the Taylor minimum-energy relaxed state, thus reducing fluctuations and improving plasma confinement. In addition, more of the initial magnetic flux should be captured in the discharge, thus increasing the magnetic field strength of the spheromak.

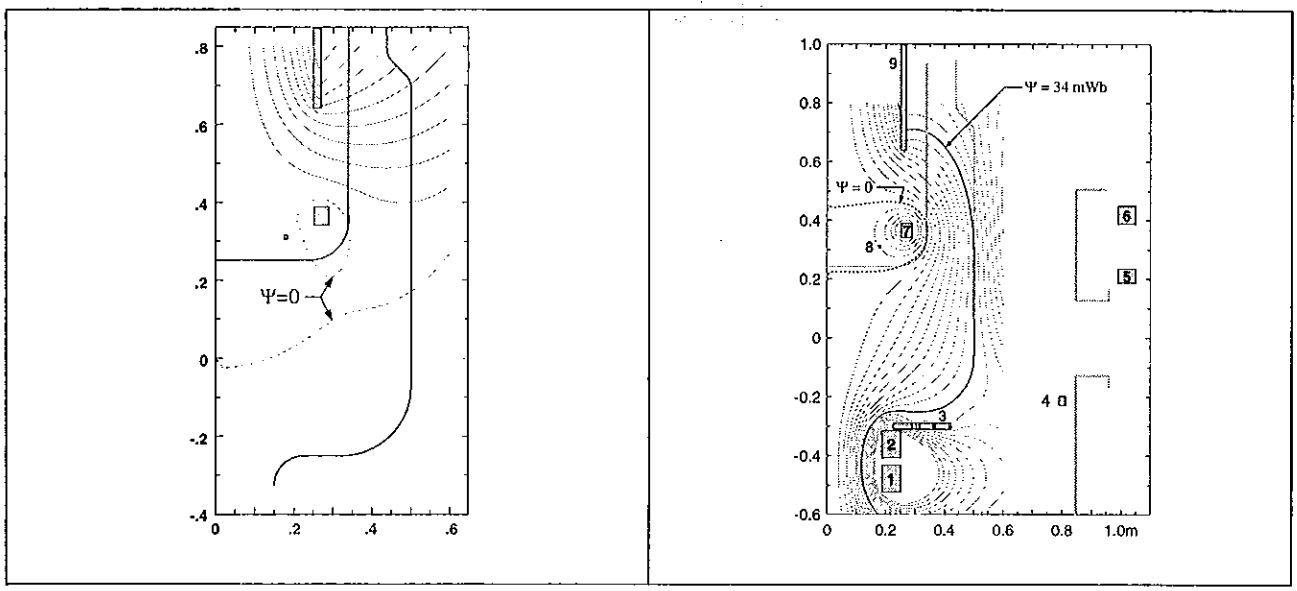

Fig. 4. Vacuum magnetic field geometries for SSPX with the standard coil set (left) and with the bias field coils (right).

The goals for the LDRD project, were then to:

- Install and operate a set of six, independently controllable, bias magnetic field coils to produce flexible vacuum magnetic field configurations in the SSPX spheromak.
- Use the bias coils to lower the spheromak formation threshold current in order to better match the injector λ to the spheromak λ.
- Compare the magnetic field generation efficiency between flux core and standard Marshall-gun injector geometries.
- Use Thomson scattering to measure the electron temperature to compare the energy confinement time in plasmas with and without the use of the bias magnetic field coils.

These goals were important for demonstrating progress on developing the spheromak concept. As such, they are related to the broader LLNL spheromak program funded by the USDOE. The construction and operation of the SSPX facility is funded by the DOE Innovative Confinement Concepts Program, which is aimed at developing alternate paths to fusion power besides the tokamak, which is the present leading candidate for a magnetic fusion energy power reactor. The Office of Fusion Energy Science has defined a development path for concepts that begins at the "Concept Exploration " phase. At this level, experiments are funded for periods of 3–6 years at the $3–5M/yr level in order to address a very limited set of questions fundamental to making the concept work. As stated above, global energy confinement scaling is the key issue for the spheromak.

In the remainder of this report, we summarize the results of this project in terms of meeting our objectives.

3. Overview of the SSPX Spheromak

The SSPX spheromak device was designed and built at LLNL. It began operating in April 1999. The device is similar to other coaxial injection spheromaks such as CTX [5] and SPHEX [6], but several significant improvements have been incorporated into the design, including a conformal flux conserver shape to minimize open field lines, a flexible magnetic geometry, and a large-radius injector to increase drive efficiency. State-of-the-art vacuum techniques (high temperature bake, glow discharge cleaning, titanium gettering, and helium shot conditioning) have been used throughout to minimize impurities in the plasma [7]. Figure 5 shows a cross section of the device before the bias field coils were installed and labels the main components: vacuum tank, flux conserver, inner electrode, and outer electrode. A reference MHD plasma equilibrium generated by the CORSICA code [8] is included.

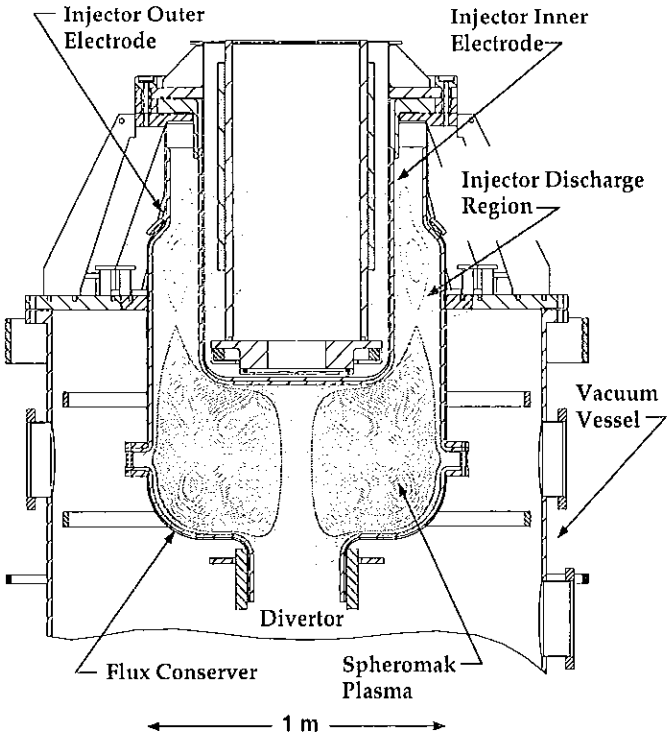

Fig. 5.SSPX spheromak and vacuum vessel, showing the helicity injector (inner and outer electrodes) flux conserver, injector coils inside the injector inner electrode, bias field coils and representative spheromak plasma magnetic flux surfaces calculated by the CORSICA code.

The SSPX device routinely operates with pulse lengths up to 3.5msec and injector currents up to 550kA. Peak edge magnetic fields of 0.25T have been obtained and plasma electron temperatures greater than 150eV have been measured. Typically, the plasma density is in the

range 0.5–1.5×$10^{20}$$m^{-3}$. So far, we have fired about 2500 plasma pulses since the installation of the bias field coils, with about half of these using some combination of the coils.

We measure the plasma parameters using a growing set of plasma diagnostics. Over 120 data channels are acquired after each plasma pulse. The chord-average plasma density vs. time is measured by a CO2 (10.6mm) interferometer, while profiles of plasma density and temperature at a single time point are obtained by a 10 channel Nd:YAG Thomson scattering system. The plasma magnetic fields are measured by an array of magnetic pickup coils mounted in the flux conserver and currents flowing in the flux conserver are measured with an array of 14 Rogowski coils mounted on current shunts spanning the midplane diagnostic slot. Total radiated energy is measured with a bolometer and impurity line radiation is monitored with a VUV spectrometer and two tunable monochrometers.

The time history of a typical SSPX discharge is shown in Fig. 6. A 10kV capacitor bank drives the initial spheromak formation with currents as high as 450kA. The edge magnetic field rises over about 300μsec to about 0.22T at the midplane. The toroidal magnetic field in the plasma is about 1.5 times the injector current. The plasma density decays from more than

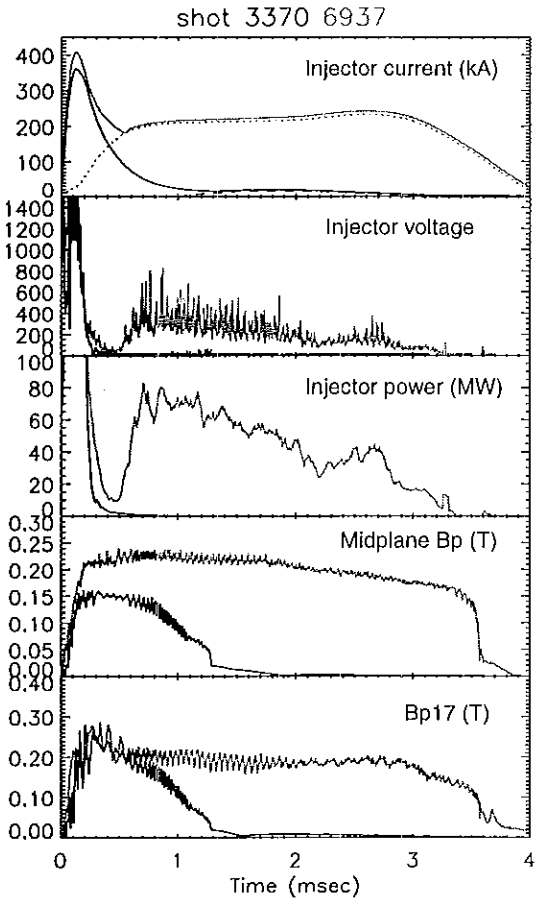

Fig. 6. Representative SSPX discharges without bias coils. Black-formation bank only. Red–with sustainment bank.

2×$10^{20}$$m^{-3}$ to about 5×$10^{19}$$m^{-3}$. After initial formation, the plasma either decays away by

resistive dissipation (black traces) or is sustained by a current pulse from a second, larger bank for periods up to 3.5μsec (red traces). The current is maintained nearly constant through the use of a pulse-forming network attached to the sustainment bank. Peak electron temperature during sustainment is about 120eV. Comparison between these standard discharges and those using the bias coils will be presented in Section 4.

2.1 Bias Coil Installation and Testing

The SSPX bias magnetic field coils were designed to produce a vacuum magnetic configuration that threaded the flux conserver and minimized the amount of flux intersecting the flux conserver in the main chamber. The location, number of turns per coil, and current in each coil was determined using the CORSICA code to compute and plot the resulting vacuum magnetic field contours as in Fig. 4b. A number of coil configurations were examined before the final set of six was selected. In the end, the field lines remained parallel to the flux conserver to within about 2mm throughout the volume. Further constraints were that the current density for each coil had to match commonly available conductor materials and the operating voltages and currents had to match surplus power supplies already on hand at LLNL. Thermal considerations were also important for the four magnets installed inside the vacuum vessel.

The four magnets inside the vacuum vessel were surrounded by a vacuum jacket to allow isolation between the magnet and the SSPX vacuum in case leaks in the cooling system developed. This design also eliminated the need for high current vacuum feedthroughs since the magnet leads remained isolated in a flexible umbilical conduit. An outside vendor built the magnets. The photo in Fig. 7(a) shows coils 1–3 in their vacuum jacket before installation in SSPX. Fig. 7(b) shows them as finally mounted to the spheromak. The magnets were mechanically aligned to the SSPX vacuum vessel and flux conserver since the cost of making more accurate magnetic field measurements was prohibitive. The total cost of the magnet assemblies was about $150,000, excluding installation.

The new bias coils are powered by six Alpha Electronics 800A power supplies, which are programmed by the main SSPX control computer. The polarity and current in each coil can be separately adjusted as needed to produce the desired magnetic field configurations. Before operation started we separately tested the power supplies using a dummy load and we verified the direction and magnitude of the fields using a Hall magnetic field probe. During

testing we also characterized the heating of the coils and determined the operational limits. The control computer monitors the temperature of each coil by calculating the circuit resistance during each pulse; the operational limit has been set to 150C by the specs of the winding insulation.

During testing we also discovered a leak from the cooling channel to the vacuum jacket for two of the internal coils. We reduced the leak rate to acceptable levels by adding standard automotive stop leak product to the cooling circuit and heating the water to 90C for eight hours. Since then, the magnets have performed according to design specs. The complete task of installing and testing the coils and power supplies required a total of about six months.

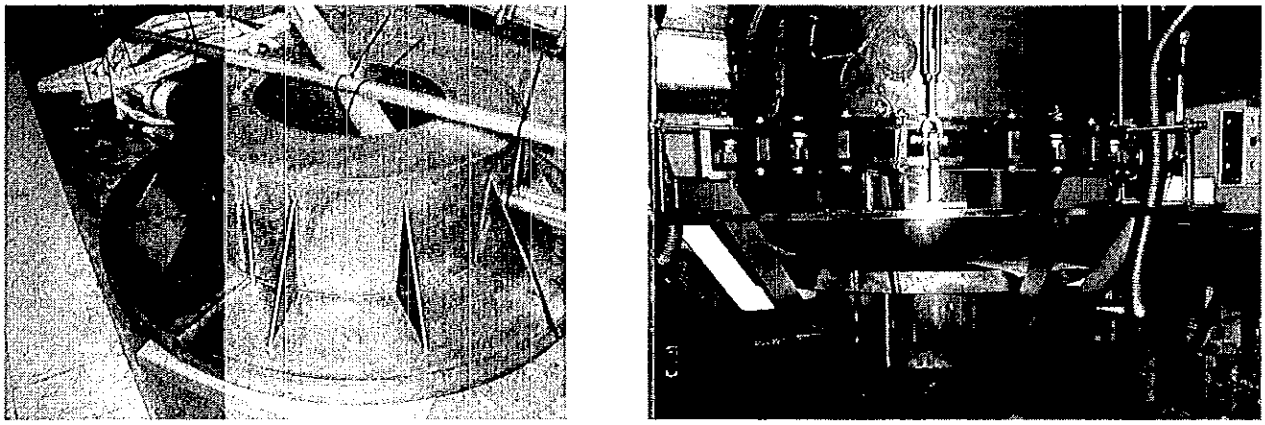

Fig. 7. Bias coils 1–3 ready for installation (RHS) and installed on flux conserver (LHS).

3.2 Bias Coil Operation

The bias coils allow a wide range of magnetic field configurations to be produced. So far, we have explored about eight different cases going up to the full design flux of 34mWb in several of them. Six of the eight cases are shown in Fig. 8 below. Variations of these cases have also been run in experiments. Operationally, using the bias coils has generally opened up parameter space for SSPX, allowing us to form spheromaks with a lower ratio of gun current to flux (i.e., λ_g) than for the reference case. The bias coils have also allowed us to operate with lower gas prefill and hence lower plasma density, than before. Without the bias coils, we needed to puff in about 2 Torr-liters of hydrogen to obtain electrical breakdown in the injector and to form a spheromak. Now, we can break down and form spheromaks with less than

0.5 Torr-liters of hydrogen. This allows us to obtain very low-density plasmas ($n_e \leq 2\times10^{19} m^{-3}$). Low-density operation provides a window to obtaining higher electron temperatures, as will be discussed below.

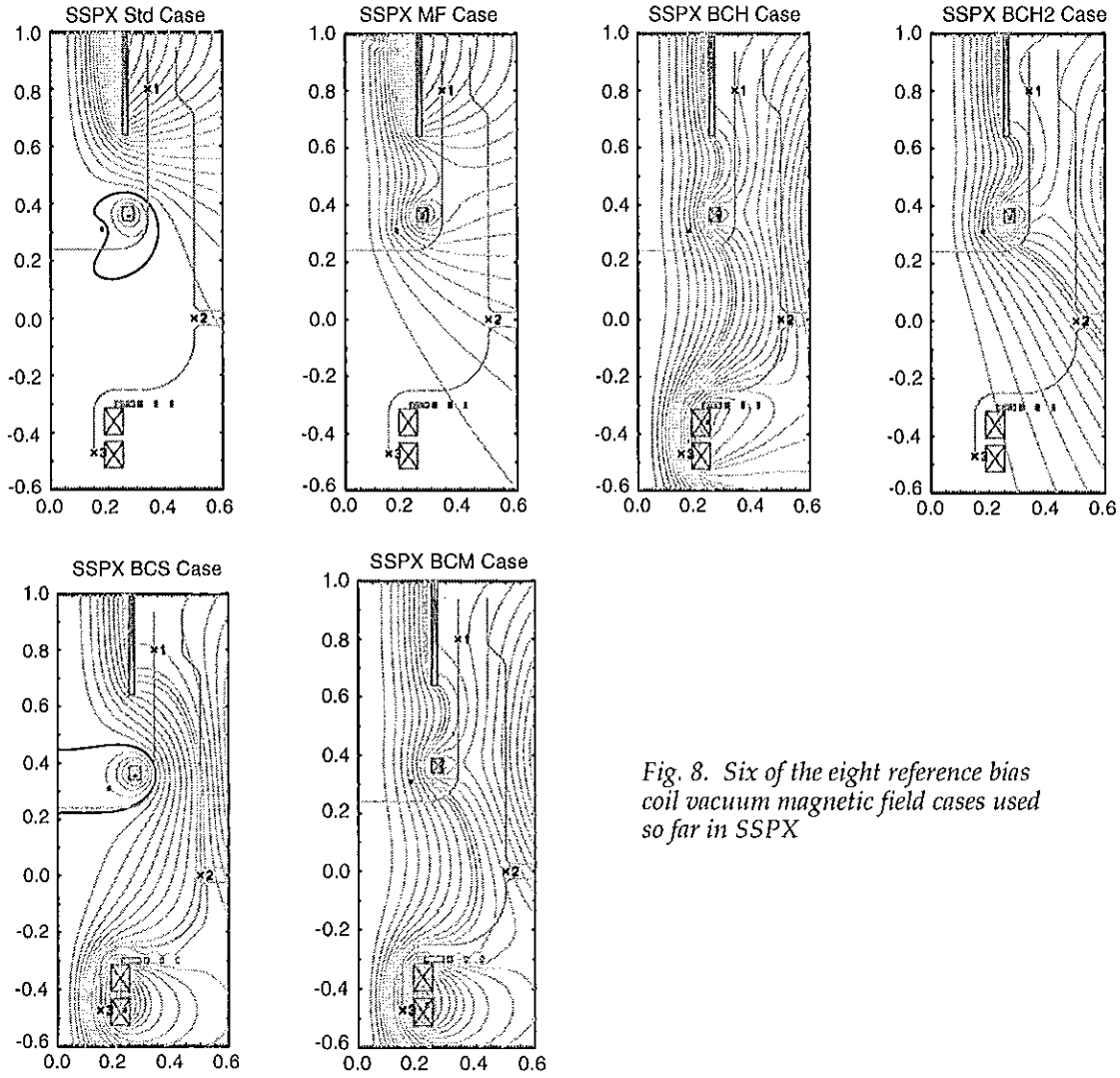

Fig. 8. Six of the eight reference bias coil vacuum magnetic field cases used so far in SSPX

Three of the bias coil configurations we have run (BCH, BCS, and BCM in Fig. 8) cause most of the discharge current to exit the bottom of the flux conserver, where we installed a solid divertor plate. Initially, this plate was stainless steel, but we found that a significant fraction of the input energy was deposited on the plate, causing surface melting. This, in turn, introduced impurities into the plasma, raising the density uncontrollably and causing significant radiation loss and plasma cooling. Figure 9 shows the radiative losses for three groups of shots, one with the bias coils that showed divertor melting, and two without the bias coils showing a low radiation fraction. To improve the situation, the stainless steel plate was

replaced with one made from molybdenum; so far we haven't seen the same uncontrolled rise in density. However, we sometimes still signs of Mo radiation in the VUV spectra, so we are considering a new cylindrical divertor plate design that will maximize the contact area and minimize the peak heat flux on the divertor when operating with the bias coils.

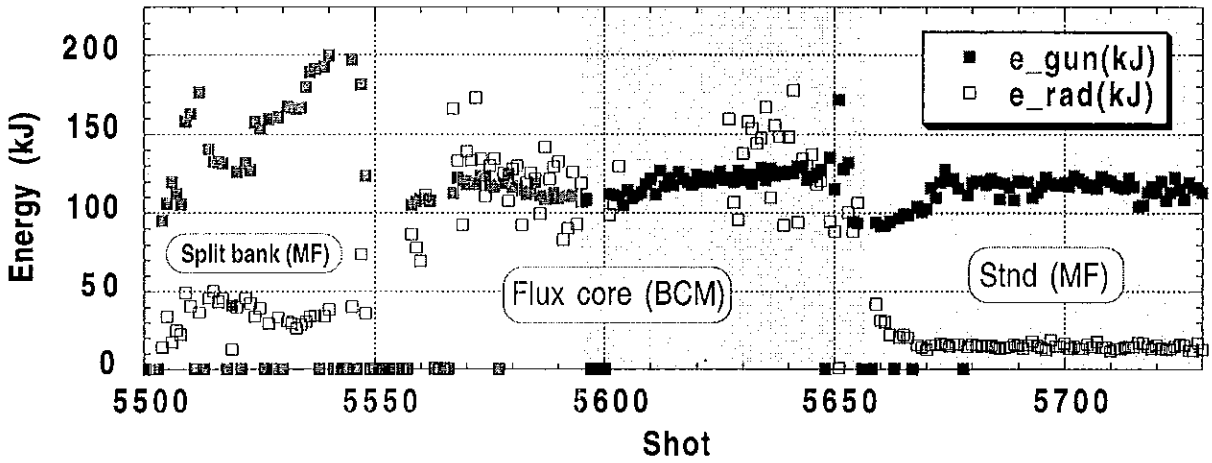

Fig 9. Radiative energy loss (e_rad) compared to input energy (e_gun) for three groups of SSPX discharges. The center region, labeled BCM, is with bias coils, while the other two are without.

4. Experimental Results

In this Section we present the results from experiments using the new bias coils, along with other hardware and diagnostic upgrades installed on SSPX. The newly obtained magnetic field flexibility is central to these results. Reported here are T_e measurements in new magnetic flux geometries, results from sustainment experiments, and power balance modeling of buildup.

4.1. Electron Temperatures in SSPX

In a nearly sustained discharge in modified flux (partial flux core geometry) with modest gun current ($\lambda_g/\lambda_0 \approx 1$) during sustainment, Thomson scattering has measured n_e and T_e profiles peaked near the magnetic axis (T_{e0}=120 eV, n_{e0}=1x10^{20} m^{-3}, and β_{e0} *(local)*~5%). Here, ϕ_g is the gun flux, $\lambda_g=\mu_0 I_g/\phi_g$, and λ_0 =10 m^{-1} is the flux conserver eigenvalue. Within measurement errors, these profiles depend on the poloidal flux, computed from CORSICA equilibrium fits to a wall poloidal magnetic probe array [8]. They are consistent with good confinement flux surfaces or very long field line connection lengths to the wall (~100 m). Low magnetic turbulence, preserving good flux surfaces, was probably important for these results.

Using the bias coils to vary magnetic flux geometry, the injected gas required for breakdown and spheromak formation was reduced a factor ~6. Preliminary investigations explored flux core geometries and a case with the limiting flux boundary surface parallel to the wall. This extends the density range during sustainment from n_e~10^{20} m^{-3} down to ~$0.2x10^{20}$ m^{-3}, resulting in a large increase in core T_e at lower density shown in Fig. 10. In the plot density was divided by the square of the poloidal field at the midplane wall and B_n=B_p/0.2 was normalized to 0.2 T. Whether this data is evidence of a beta limit is under investigation. Measurement errors in T_e at lower density are uncertain because of plasma bremsstrahlung. Diagnostic improvements are underway.

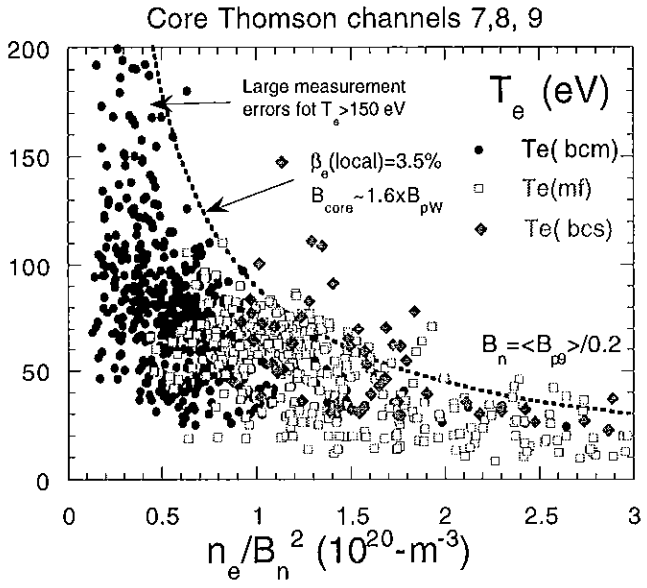

Fig.10 Accessible range of core T_e and n_e for several vacuum flux geometries. B_p(wall)~0.2 T is the nominal value for most discharges.

4.2. Spheromak Formation and Sustainment

SSPX experiments have investigated 1) short pulse, high current formation and 2) sustainment and buildup at longer pulse and lower current. Peak poloidal field scales directly with peak gun current (Fig. 11), using either one or two pulses (second pulse at higher current). The ratio B_p/I_g does not appear sensitive to vacuum magnetic flux geometry.

Long pulse buildup, followed by sustainment, is clearly the preferred way to obtain higher field because lower current and power are required. Asymmetric turbulent fields (with m=1), sufficiently large for dynamo current drive to buildup and sustain the plasma, must not also destroy confinement. Global-mode MHD fluctuations, observed on wall magnetic and wall current Rogowski probes, are prominent in SSPX. A kinking of central column open flux (m/n=1/1, 'dough hook') occurs during formation and sometimes during sustainment. Although spheromak magnetic field increases with this mode, large mode amplitude may not

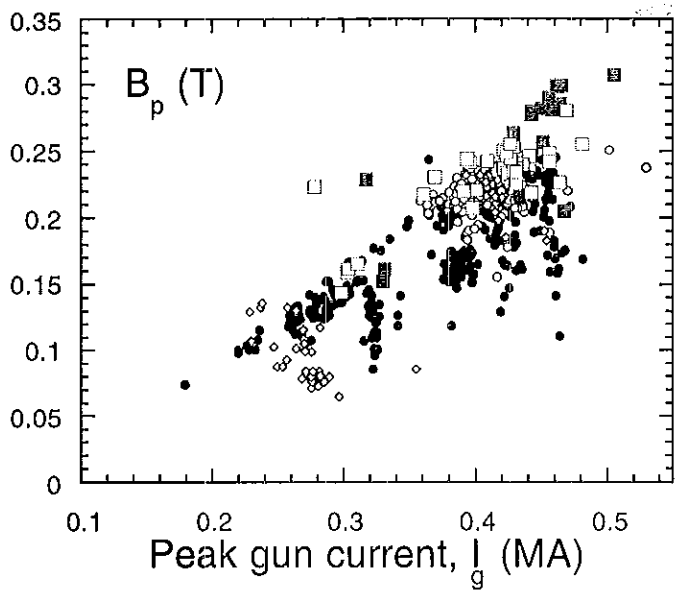

Fig. 11 Dependence of the midplane wall poloidal field on peak gun current during spheromak formation.

be favorable for good confinement. Higher order modes (m/n=1/2, 1/3, 1/4) and shorter wavelength turbulence are also seen during sustained discharges with low levels of turbulence.

Understanding buildup and the associated turbulence is the key issue for SSPX. For buildup we need to understand the relation between gun impedance, the fraction of gun power coupled into the 'good confinement' spheromak core, and the role of turbulence in core losses.

4.3 Power Coupling and Spheromak Buildup

. We have used power balance and a gun impedance model proposed by Fowler [9] to calculate buildup in SSPX. Fowler models the gun voltage as $V_{gun} = V_{sh}+V_{R(edge)}+V_{sp}$, where $V_{sh} = \gamma T_{e(edge)}$ (γ=constant) is the net gun sheath voltage drop and $V_{R(edge)}$ is the dissipative resistive voltage drop in the plasma edge. To drive the equilibrium toward the Taylor state, V_{sp} models periodic turbulent transport (by island overlap and reconnection) of inductance energy (related to current flow in the plasma edge) into the spheromak core. $V_{sp} \propto \kappa I_g[1-(I_0/I_g)^2]$ [10] is excited above a gun current threshold, $I_0=\lambda_0\phi_g/\mu_0$. The gun power coupled into the spheromak is defined by $P_{sp}=\varepsilon_P P_g$, where $\varepsilon_P=V_{sp}/(V_{sh}+V_{R(edge)}+V_{sp})$. $\varepsilon_P(I_g)$ was determined from a fit of the parameters γ and κ to measured gun voltage during sustainment for a group of SSPX modified flux discharges with fixed ϕ_g and varying I_g. Typical values are V_{sh}~150 V, ε_P ~0.2-0.3, and $T_{e(edge)}$ ~20 eV near the geometric axis.

Magnetic energy buildup was calculated from solution of $dW_m/dt=\varepsilon_P P_g - W_m/\tau_{Em}$ using gun current and voltage for a spheromak discharge. Fig. 12 compares the model and CORSICA

equilibrium fits to magnetic probe data for discharge 4325. We obtain fair agreement with CORSICA for τ_{Em}~1-2 ms. Although T_e data is unavailable for this discharge, core temperatures T_e~20-40 eV are expected at the high density (~2-3x10^{20} m^{-3}) measured by CO2 interferometry. The inferred value of τ_{Em} is consistent with Spitzer resistivity in this range of T_e.

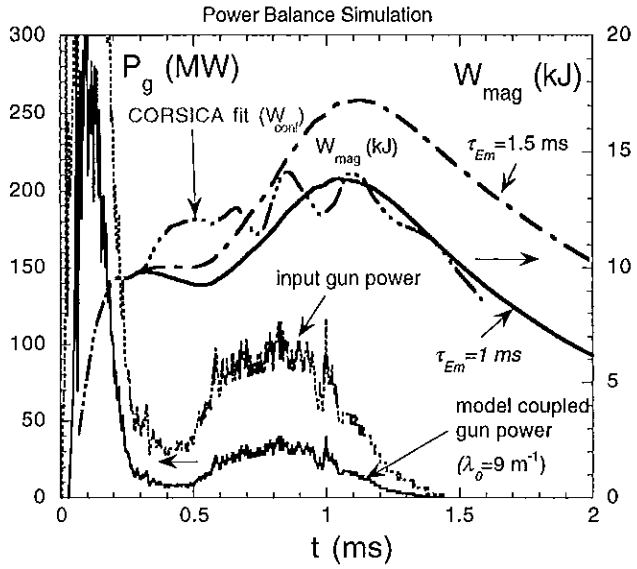

Fig.12 Core magnetic energy from CORSICA fit to magnetic probes (discharge 4325) and energy computed from Fowler power coupling model and magnetic decay time.

4.4 Beta Limits

Performance (ability to reach high temperature with low losses) of SSPX may be governed by pressure limits. The normalized plasma pressure, expressed as $\beta=nkT/B^2$, can be limited by a number of different effects, although usually pressure-driven instabilities are referred to as beta limiting. However, all instabilities tend to increase the energy and particle transport from the spheromak to the outside world, hence limit the temperature or density, and correspondingly the beta, of the spheromak. Current-driven instabilities can be avoided by careful current-profile control, while capping the temperature or density before various modes become unstable can control pressure-driven instabilities.

We are building a case to show that the spheromak is reaching a beta limit in many, if not all discharges, and identifying the instabilities that give rise to the limit. There are some specific instances that we have studied using the bias coils to control plasma density and magnetic field strength. We have also examined our global database to look for broader trends. The specific instances and trends are as follows.

Specific instances showing beta limits:

a) We have used the bias coils to produce flux configurations that give better control of the current profile. It is possible to suppress the fluctuations exhibited in the decay due to the n=2 mode by raising the edge current density (or lambda). In suppressing the fluctuation amplitude (perhaps by stabilizing the n=2 current-driven mode), we have been able to produce regimes of high beta (β_e ~6%) – the highest beta for a driven spheromak.

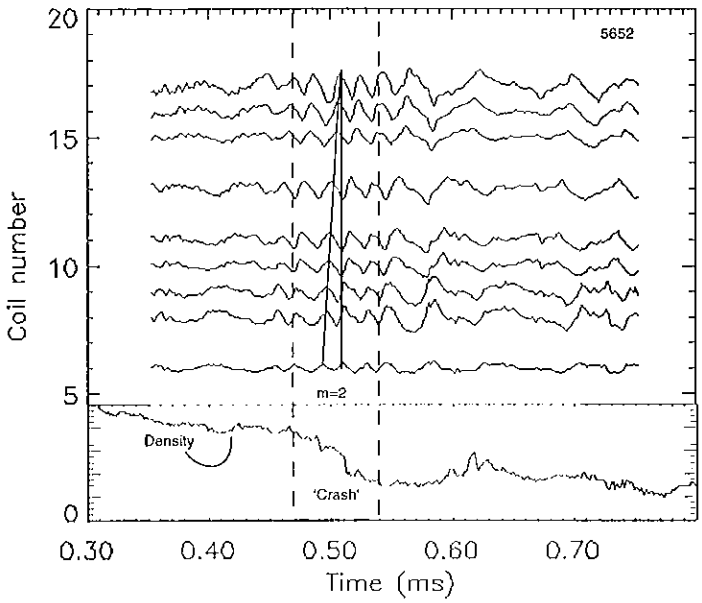

Fig. 13. Collapse in core density and onset of the m/n=2/4 mode

b) We have used the bias coils to facilitate breakdown at lower plenum pressures, giving lower density spheromaks that exhibit pressure-driven instabilities (and magnetic structures (maybe islands) with mode number m/n=2/4 (Fig. 13). These instabilities cause a rapid collapse of the core density, however, the pressure profile was measured in these discharges, and it was found that it remained the same before and after the onset of

c) instability, indicating that the discharge rapidly heated after the density collapse up to a beta limit (Figs. 13 and 14).

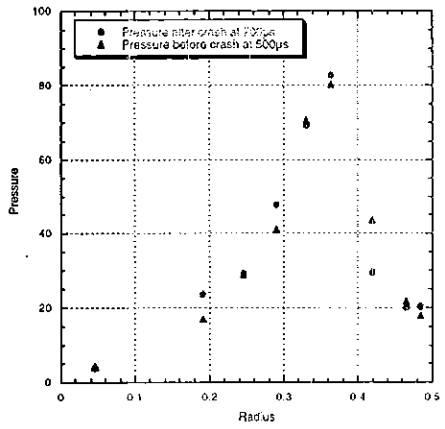

Fig. 14. Measured pressure profiles before and after the onset of instability

d) In low-density discharges, accessed with the bias coils, we have observed high-frequency, low-correlation-length magnetic field fluctuations that are not otherwise observed at higher density. The origin of these fluctuations is understood to result from pressure-driven

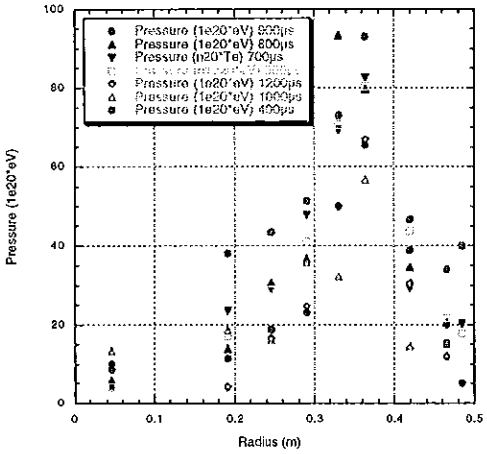

Fig. 14. a) Measured pressure profiles during a low density shot; b) same profiles normalized to the field squared (note better grouping).

modes, or the Mercier type (ballooning, or local interchange). We have compared the measured pressure profile with one that is marginally stable to the Mercier-type mode [11], and found that it agrees, although without taking the ion temperature into consideration (Fig. 15). Still, without further measurements, the Mercier-stable profile is at a higher beta than anticipated, maybe because of large shear in the magnetic field.

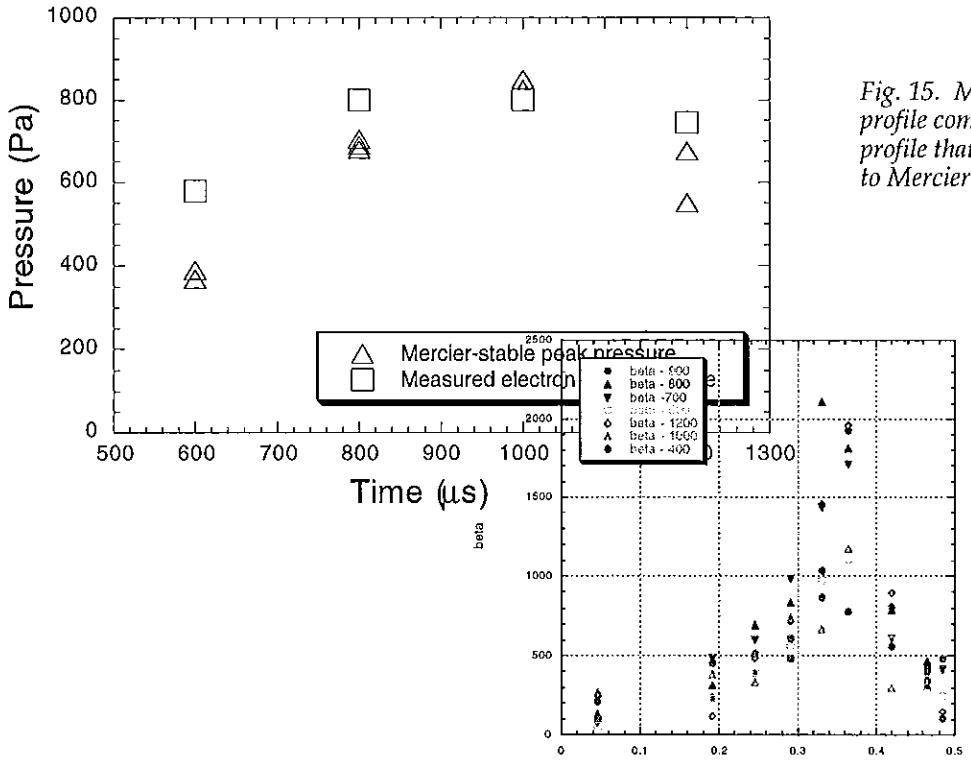

Fig. 15. Measured pressure profile compared with a pressure profile that is marginally stable to Mercier.

Trends pointing to beta limits:

a) By compiling a database of core density and temperature measurements from many shots, a clear beta-limit trend is determined. Plots of core T vs. core n/B^2 from many different discharges can be bounded by a line that is given by beta_poloidal~3%. This trend appears to be independent of the flux-configuration that is programmed with the bias coils as shown in Fig. 10 above.

4.5 Effect of Vacuum Fields on Formation and Decay

In previous spheromak experiments, applying a vacuum field have mostly resulted in poor performance. In the worst case, adding a vacuum field inside the flux conserver produced a tilt instability, which destroyed the configuration. Only moderate success was claimed for efforts to separate the spheromak from the wall. Finally, the presence of vacuum fields ('field errors') in the confinement region was understood to act as a helicity sink, and only when these were mitigated was an improvement in confinement observed. In the CTX mesh flux conserver it was observed that an electric field would develop at the edge, which would drive currents on the open field lines and increase the energy loss [12].

While we observe some negative aspects of field imposition, the presence of vacuum fields has allowed us to drive the spheromak at the edge giving better control of the current profile, and facilitated breakdown at lower density, hence giving low-density spheromaks. The following is a summary of the pertinent results from imposing a vacuum field on SSPX spheromaks.

1. Introducing 'field errors' causes the decay to be more rapid. By increasing the field-strength of the field that penetrates the bottom of the inner electrode, the decay rate of the spheromak can be increased by as much as a factor of two, as shown in Fig. 16. In discharges with 'field errors', the n=2 instability (resulting from a peaking of the current profile) is immediately onset after the drive ceases. The spheromak with field errors remains connected to the source during decay, evidenced by a reversal of the gun voltage.
2. Instability onset and rapid decay can be explained without recourse to helicity dissipation. As the injector current falls, the ejection threshold is re-reached, causing the injected current path to rapidly change from along the core of the spheromak to within the gun (evidenced by the return of the gun voltage to zero). The spheromak experiences an immediate change in the current profile and decays. The decay of the toroidal flux imposes a voltage along the open field lines (evidenced by a reversal in voltage on the source).

However, no current can be driven along the open field lines, as these are connected (through the source) to a high impedance load. The spheromak therefore retains an n=2 distortion. The large amplitude fluctuations from this mode give rise to a rapid loss of heat

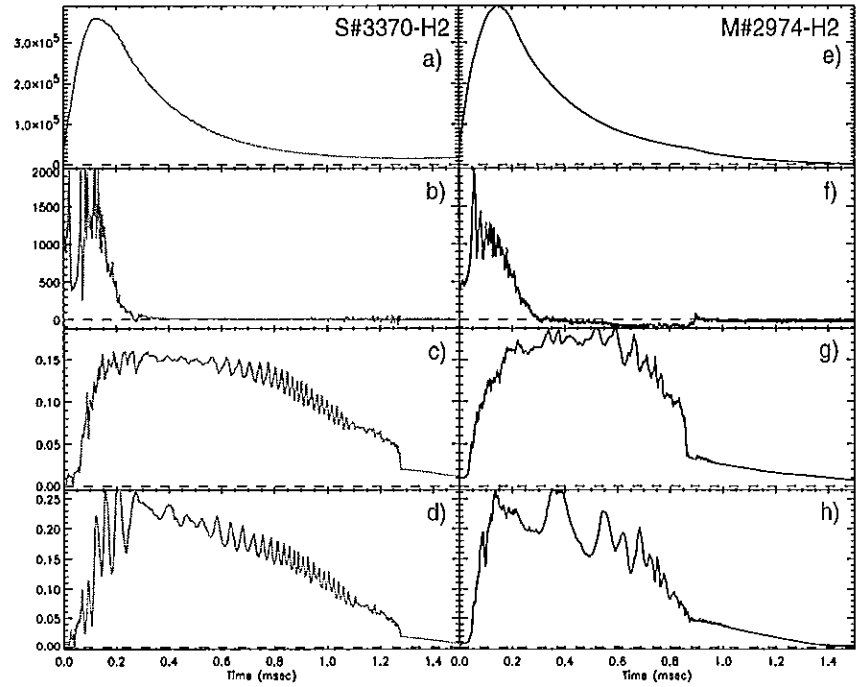

Fig. 16. Decay rate of the configuration with large field errors (e-h) is greater than that with low (a-d). Also, fluctuation amplitudes are higher, instability is onset immediately after the current switches to the gun, and spheromak remains connected to the source.

and particles and hence to a rapid quench of the spheromak through increased resistivity.

3. While the decay may be more rapid for spheromaks with imposed vacuum field, the formation appears not to be adversely affected. The field strength of the spheromak with imposed field reaches and often exceeds the field that is reached without imposed fields. It is conjectured that the higher fields result in part from an outward shift of the spheromak equilibrium (some equilibrium modeling supports this conjecture).
4. In fact, over a wide range of vacuum fields, field errors do not affect the formation of the spheromak. Despite the imposition of strong vertical fields on the confinement region, the spheromak consistently forms with a peak field at the midplane of around 0.2T for an injected current of 400kA. The field strength of the spheromak appears to be quite independent of the vacuum field configuration, implying that the helicity injection rate is independent of vacuum field configuration.
5. Field errors will allow a change in the position of the current footprint. Electrons remain well magnetized in the spheromak, and will predominately enter or leave a material boundary where **B.n**=1. Programmed vacuum fields that penetrate the surface there can

therefore facilitate a change of the position of the current footprint to the bottom of the inner electrode.

6. Field errors allow sustainment at lower currents. By changing the current footprint position, the injected current need not bend out field from the gun in order to drive the spheromak. In other words, the threshold for ejection need not be reached in order for current to enter the confinement region. This means that the configuration can be driven gently with an edge lambda that is close to the eigenvalue of the spheromak (i.e. with a flat lambda profile). Driving with a flatter profile has improved performance in SSPX by suppressing the n=2 fluctuations (and is related to PPCD in the RFP [13])
7. PTS measurements show the position of a separatrix even with strong vacuum fields imposed. Imposition of vacuum fields give rise to a 'flux-core' configuration with a discernable separatrix in profile measurements of temperature that agree well with equilibrium reconstructions. In the absence of internal field profile measurements, such a result boosts confidence that 2D equilibria are meaningful.
8. However, NIMROD [14] simulations tend to show open field configurations with imposed vacuum fields.
9. Lower density operations are feasible by producing a Penning region in the gun. Generating a Penning region in the source opposite to the gas valves assists breakdown at low plenum pressure. Low-density operations have since given the highest temperatures in the spheromak.

4.5 Energy Confinement in SSPX

We determine the energy confinement time in SSPX using the following methodology. First, CORSICA is used to compute the plasma equilibrium (current density profile, shape of flux surfaces, location of the separatrix, etc.). Then, using the measured density and temperature profiles, we compute the total stored energy and the ohmic heating input power. From these results we can compute both the energy confinement time $\tau_E=(\int nkT)/P_{ohmic}$ and the local radial energy transport coefficient from the local heat flux. We assume classical Spitzer resistivity proportional to $Z_{eff}/T^{3/2}$, with $Z_{eff}=2.3$ and assumed constant everywhere. In the earlier estimate, we did not compute the ohmic heating power on the open field lines, but now Dick explicitly calculates ηj^2 on the open field lines as well. On these open field lines we set T_e to the electron temperature at the separatrix.

We fit the electron temperature data from the Profile Thomson Scattering System to a smooth spline curve. The number of knots in the spline fit is user selectable: we have tried between 4 and 8 (the higher the number of knots, the better the fit will pass through peaks and valleys in the data, but the more "unphysical" the profiles may look). For our most recent analysis, we created a dummy data file for SSPX shot 4624, which was actually built from many single point measurements acquired over the course of a single day of SSPX ops. More recent data provides complete profiles in a single shot, but the profiles don't appear as smooth.

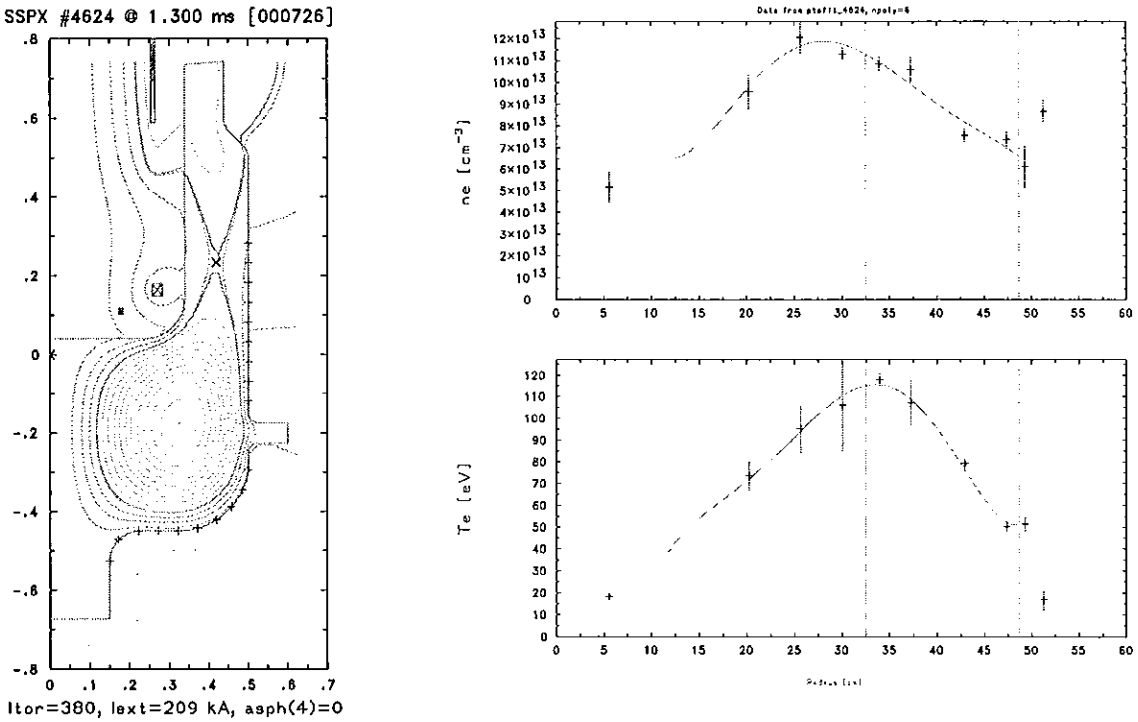

Fig.17. Model discharge equilibrium and measured n_e and T_e profiles.

We used a MHD reconstruction of discharge 4624 at 1.3msec to compute the confinement time. Several different current ($\lambda=j/B$) profiles were used, including a flat $\lambda(\Psi)=\lambda_0$, linear $\lambda(\Psi)=\lambda_0(1+a\Psi)$ with a=-0.26, and the more usual $\lambda(\Psi)=\lambda_0(1+a\Psi^{10})$. As expected, those equilibria with more current in the edge and SOL (open field line) plasma have higher ohmic heating power and correspondingly lower global energy confinement times. A picture of the equilibrium shape, assuming a flat λ profile, is shown in Fig. 17(a). Figure 17(b) shows the Thomson scattering data and the spline fit used to map the data onto magnetic flux surfaces for this shot.

The Thomson scattering data is used to fill in the plasma density and temperature on flux surfaces (assuming they are flux-surface quantities). From these data and the local current

density associated with the plasma equilibrium, the ohmic heating power can be computed on both the open and closed flux surfaces. On the open field lines, a straightforward volume integral of ηj^2 is computed, whereas on the closed flux surfaces, the flux-surface average quantities are used. Two dimensional plots of the ohmic heating power (MW/m^3) and radially-weighted ohmic power ($2\_R \times P_{oh} dA$, with dA=drdz from the CORSICA mesh) are shown in Fig. 18.

The resulting global confinement time, integrated (0 out to _=r/a) ohmic heating power, and electron thermal diffusivity appear in Fig. 19. The thermal diffusivity at the core is unchanged from our earlier calculation, as is the confinement time (see previous memo for caveats on its meaning). On the edge however, the ohmic heating power is lower on a given flux surface than in our earlier calculation. This leads to a significant (factor of four or more) decrease in diffusivity and a corresponding increase in the global confinement time, from 100 to 150_sec. A more peaked current profile can raise the global confinement to 200_sec. All these calculations are subject to uncertainty in Z_{eff} profiles and to the presence of any anomalous resistivity due to fluctuations.

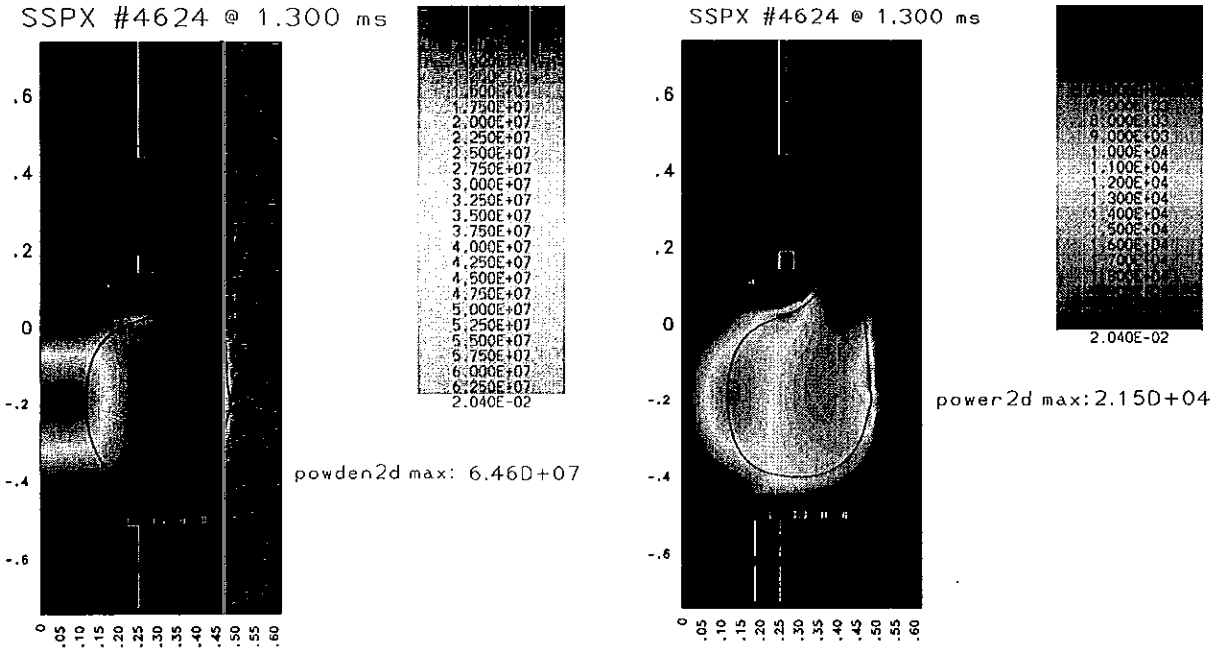

Fig. 18. Ohmic heating power density (W/m^3) and $2\pi R \times$ power density assuming Z_{eff}=2.3 and using $\lambda=\lambda_0= 9.5m^{-1}$.

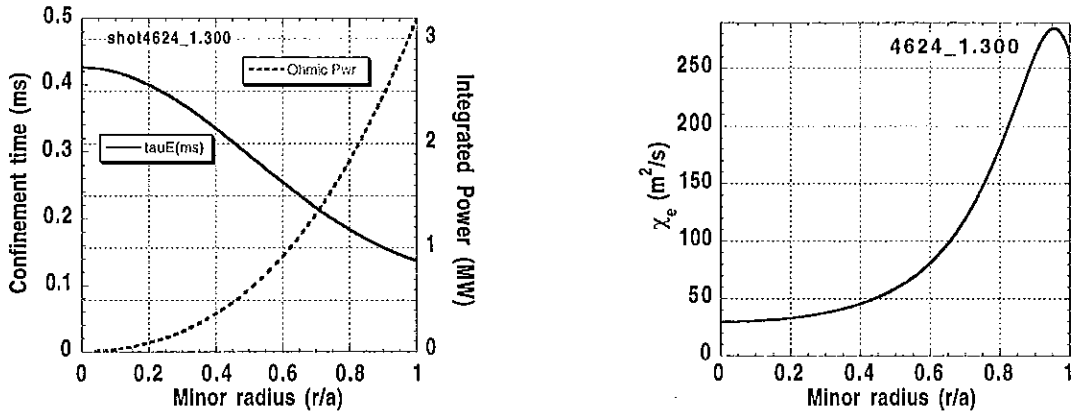

Fig. 19. Electron energy confinement time, integrated ohmic input power, and electron thermal diffusivity as computed from the CORSICA/Caltrans equilibrium and PTS data above.

We have neglected the ion contribution to the total stored energy for the confinement time calculation because we know so little about the T_i profile. From measurements of the Doppler broadening of an Oxygen V line at 2781Å we find that T_i is quite high at first, during buildup. However, during the sustainment phase, T_i seems to average about 100eV, which is close to Te for these sorts of plasmas. If we assume that the ions are heated by collisions with electrons, then we should include them in our estimate of the total plasma thermal energy, which would double the energy confinement times reported here. However, if the ions are heated directly by fluctuations, then we should add this input to the ohmic power, and the confinement time would remain unchanged. Finally, if the ions are hotter than the electrons, we should add an exchange term to the ohmic heating power, so the electron energy confinement time would be reduced. Clearly, some idea of the T_i profile would be helpful, though we would still be left in the dark regarding the contribution of turbulent ion heating.

We expected to be able to compare the energy confinement time between the various magnetic configurations, but so far we have been limited by poor S/N in the Thomson scattering data for some of better discharges. This results from higher than expected plasma radiation at 1mm. We are now working to increase the Nd:YAG laser power so that we can obtain these important data.

We can, however, predict the scaling of confinement time with core and edge temperature using the CORSICA code. We expect that the core confinement would increase with electron temperature something like $W/P_{OH} \propto n_e T_e^{5/2}$, a very strong dependence indeed! Using CORSICA with model Te and ne profiles for form similar to the experimental data,

$$T_e(r) = (T_0 - T_{edge})\sqrt{1-(\tfrac{r}{a})^{\alpha_T}} + T_{edge} \quad \text{and} \quad n_e(r) = (n_0 - n_{edge})\sqrt{1-(\tfrac{r}{a})^{\alpha_n}} + n_{edge}\,. \qquad (4)$$

we computed the global confinement time for SSPX-like plasmas. Here a is the minor radius of the plasma (distance from magnetic axis to outboard separatrix). The measured T_e data seem to correspond to the case of α_T near unity, but the script allows for arbitrary profile shapes and

user-selectable ranges for the core and edge temperatures. For this study we used a fixed MHD equilibrium (4624) with a flat λ profile for the results shown here. Again, we assumed Z_{eff}=2.3.

Results from the CORSICA/Caltrans modeling appear in Fig. 20. The computed confinement time rises with central electron temperature, from about 50μsec at 50eV to 420μsec at 300eV, as shown in (a). At the same time, the ohmic heating power on closed field lines decreased from 6 to 1.9MW. In this case, the edge temperature was held fixed at 40eV, which may not be unreasonable for hotter plasmas. If we scan the edge temperature instead, and leave the peak core Te fixed at 200eV, we obtain the data of (b) on the right. From the figure, we see that increasing the edge T_e from 40 to 100eV can almost triple the global confinement time.

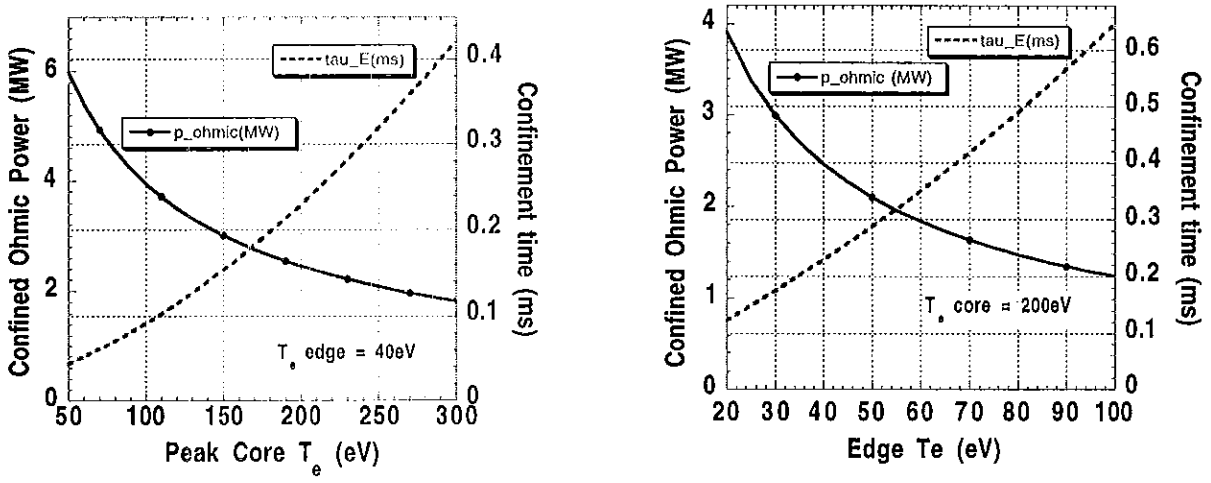

Fig. 20. Scans of core and edge temperature. α_T=1.0, T_{edge}=40eV in (a), T_{core}=200eV in (b).

From these results, we may postulate what effect auxiliary heating would have on the core electron temperature. If we assume that the density and confinement time remain fixed (pessimistic if χ_e scales as $S^{-\alpha}$), then we can write down a simple expression for the peak temperature in the core vs. applied auxiliary heating power, P_{rf}:

$$T_{rf} = \left(\frac{P_{OH} + P_{rf}}{P_0} \right) T_0$$

where P_0 is the initial ohmic heating power within the region of interest and $P_{oh}=P_0T^{-}$

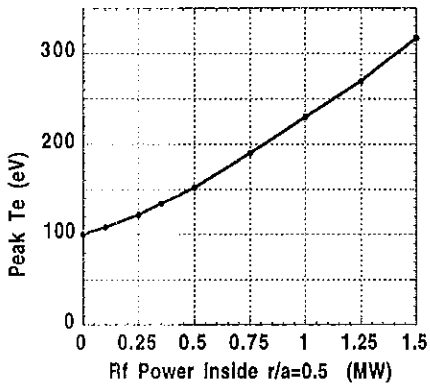

Fig. 21. Peak core T_e vs applied RF heating power inside r/a=0.5, assuming P_{oh}=0.5MW from the CORSICA/Caltrans analysis in Fig. 3

$^{3/2}$ is ohmic heating power at plasma temperature T. In this case, if we choose r/a=0.5, we have P_0=0.5MW. Using T_{e0}=100eV, we predict that the peak T_e vs. RF heating power deposited would scale as shown in Fig. 21. For this very simple prediction, we assumed that, as the plasma heats, the ohmic heating power falls as $T^{-3/2}$.

5. Future Directions

Recently, we have developed a new magnetic configuration using the bias coils (BCB), which allows steady field buildup throughout the discharge. This magnetic configuration has a low threshold current due to pulling field lines out of the injector, like the modified flux case of Fig. 8. The key element, however, seems to be slowing the ramp-up of injector current, which we accomplish by starting with only a very minimal energy pulse from the formation bank. The time history for one of these discharges is shown in Fig. 22. Note that the field strength and total helicity content rise steadily until the current from the sustainment capacitor

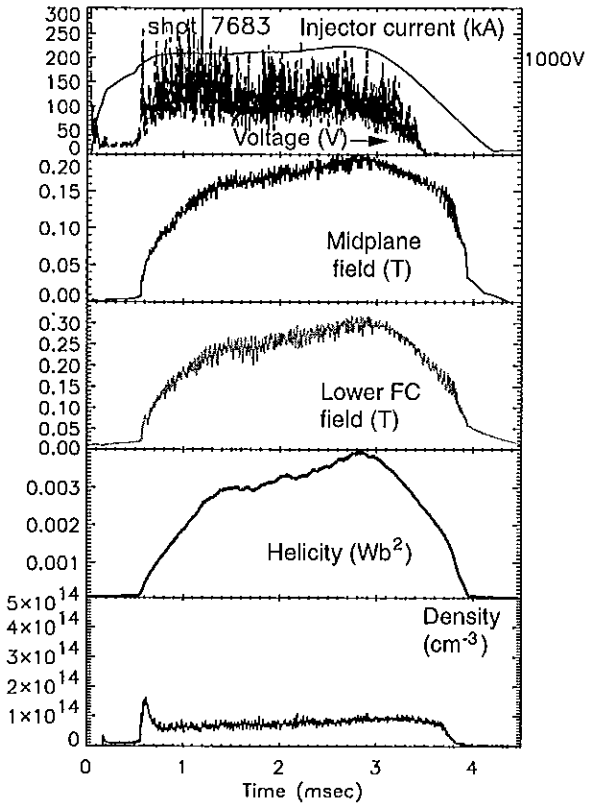

Fig. 22. Sustained field buildup using very slow formation (no large formation current pulse at the start of the discharge). Note the large injector voltage and the steadily rising helicity content.

bank begins to drop at about 3msec. All during the buildup the injector λ remains just above the flux conserver λ; i.e., the discharge is being driven just above the threshold current. Large fluctuations in injector voltage imply large changes in plasma inductance and produce a steady rate of helicity injection ($dK/dt=-2V_g\phi_g$). Unfortunately, we were not able to measure

the evolution of the electron temperature during the buildup due to high background light levels.

In the future, we plan to install probes in the injector region to measure the current density and magnetic flux contours. These data will help us correlate the field buildup with the helicity injection rate for the various magnetic field configurations produced by the bias coils. In addition, we are upgrading the Thomson scattering system (increasing the laser power and taking steps to reduce the background light) to obtain better electron temperature measurements.

In summary, the bias magnetic field coils have opened up a wide operating space previously unobtainable in spheromak experiments. This is allowing us to explore the physics of helicity injection and field build in new and unique ways. Our goal is to use these data to benchmark present MHD models for helicity injection so that we can better predict the performance of future spheromak experiments.

References

1. Woltjer, L. Proc. Nat. Acad. Sci USA **44** (1958); also Okabayashi, M. and Todd, A.M.M, Nucl. Fusion **20**, 571-577 (1980).
2. Taylor, J.B., Phys. Rev. Lett. **33** (1974).
3. Cowling, T.G. Monthly Notices Roy. Astron. Soc. **94**, 39 (1934).
4. Brown, M.R. and Martin, A., Fusion Technol. **30**, 300 (1996).
5. Jarboe, T.R., Barnes, C.W., Henins, I. Hoida, H.W., Knox, S.O., et al., Proc. 10th IAEA Conf. Controlled Thermonuclear Fusion Research (1984)
6. Rusbridge, M.G., Gee, S.J., Browning, P.K., et al., Plasma Phys. Control. Fusion **39** (1997).
7. Wood, R.D., Hill, D.N., Hooper, E.B., *et al.*, J. Nucl. Mater. **290-293** (2001).
8. Hooper, E.B., Pearlstein, L.D., Bulmer, R.H., Nucl. Fusion **39**, 863 (1999).
9. Fowler, T.K., Hua, D., J. Fusion Energy **14** (1995).
10. Barnes, C.W., Jarboe, T.R., Marklin, G.L., *et al.*, Phys. Fluids B **2**, 1871 (1990).
11. Fernandez, J.C., Jarboe, T.R., Knox, S.O., Nucl. Fusion **30** (1990).
12. Fernandez, J.C., Barnes, C.W., Jarboe, T.R., *et al.*, Nucl. Fusion **28**, 1555 (1988)
13. Chapman, B.E., Biewer, T.M., Chattopadhyay, P.K., *et al.*, Phys of Plasmas **7**, 3491 (2000).
14. Glasser, A.H., Sovinec, C.R., Nebel, R.A., *et al.*, Plasma Phys. Cont. Fusion **41**, A747 (1999).

Appendix 1. Recent Spheromak Publications

1. D. N. Hill, R. H. Bulmer, B. I. Cohen *et al.*, "Spheromak Formation Studies in SSPX," in *18th International Atomic Energy Agency Fusion Energy Conference* (IAEA, Sorrento, Italy, 2000).
2. C. T. Holcomb, T. R. Jarboe, A. T. Mattick *et al.*, "Nonperturbing field profile measurement of a sustained spheromak," Rev. Sci. Instrum **72**, 1054 (2001).
3. E. B. Hooper, R. H. Cohen, D. D. Ryutov, "Theory of edge plasma in a spheromak," J. Nucl. Mater. **278**, 104 (2000).
4. H. S. McLean, A. Ahmed, D. Buchenauer *et al.*, "Plasma diagnostics for the sustained spheromak physics experiment," Rev. Sci. Instrum. **72**, 556-561 (2001).
5. Y. Roh, C. W. Domier, N. C. Luhmann Jr., "Ultrashort pulse reflectometry for electron density profile measurements on SSPX," Rev. Sci. Instrum. **72**, 332 (2001).
6. R. D. Wood, D. N. Hill, E. B. Hooper *et al.*, "Particle Control in the Sustained Spheromak Physics Experiment," J. Nucl. Mater., **290–293**, (2001).
7. D. Buchenauer, B. E. Mills, R. D. Wood *et al.*, "Characterization and conditioning of SSPX plasma facing surfaces," J. Nucl. Mater., **290–293**, (2001).
8. Z. Wang, G. A. Wurden, C. W. Barnes *et al.*, "Density and Ha diagnostics and results for the sustained spheromak physics experiment," Rev. Sci. Instrum. **72**, 1059 (2001)
10. S. Woodruff, D.N. Hill, C.T.Holcomb, E.B.Hooper, H.S.McLean, B.W.Stallard, R.D. Wood, R. Bulmer, B.Cohen, L.LoDestro "Sustainment of a Spheromak by DC Helicity Injection," Conference proceedings, 27th EPS Conference on Controlled Fusion and Plasma Physics, Budapest, 2000
11. B.W. Stallard, D.N. Hill, C. Holcomb, E.B. Hooper, *et al.*, "Sustainment of Spheromak Plasmas in SSPX," Proc. 28th EPS Conference on Controlled Fusion and Plasma Physics, Madeira, 2001. UCRL-JC-142297 June 11, 2001.
12. H. S. McLean, S. Woodruff, E. B. Hooper, R. H. Bulmer, D. N. Hill, *et al.*, "Suppression of MHD fluctuations leading to improved confinement in a gun-driven spheromak." UCRL-JC- 144279, July 15, 2001. Submitted to Phys. Rev. Letts.

Appendix 2. Collaborations

There are several experiments currently underway in the US that provide information on resistive MHD in related configurations. We are working with these groups to ensure that we obtain the broadest possible understanding of the data.

There are three experiments which are explicitly studying magnetic reconnection: Prof. M. Brown at Swarthmore is forming pairs of small spheromaks and examining the reconnection layer between them. Dr. M. Yamada at Princeton Plasma Physics Laboratory has been studying colliding spheromaks and using the measurements to examine the behavior of reconnection. Prof. P. Bellan at Cal Tech is generating high current arcs which mimic solar flares, including effects of reconnection and magnetic helicity. He is also sending a graduate student with a high speed camera and viewing optics to observe the formation of SSPX plasmas.

Small spheromaks are formed and accelerated to high speeds (many km/s) for injection into tokamak plasmas for fueling. The primary US effort in this area is by U. C. Davis and located in the same LLNL building as SSPX. There are related efforts in Japan.

Reversed field pinches are a magnetic field confinement geometry which is limited by resistive MHD modes similar to those in the spheromak, although with a different magnetic geometry. The primary effort on RFP's in the US is the MST at the University of Wisconsin at Madison, and a larger device is operating in Padua, Italy. We have a collaboration with the MST group to use their spectrometer on SSPX to examine plasma impurity content, as well as apply their turbulent transport diagnostics on SSPX at the appropriate time, in order to provide easily compared data on transport in the presence of magnetic turbulence

The University of Washington is supplying a graduate student who has built and is now operating a Transient Magnetic Probe to measure the magnetic field in the spheromak. Besides the student, Prof. T. Jarboe provides significant physics support as well.

We are also developing a collaboration with Florida A&M university. They have proposed installing a diagnostic based on laser-induced fluorescence to measure the properties (frequencies and correlation lengths) of density fluctuations in SSPX.